Proceedings of the 7th JFPS International
Symposium on Fluid Power, TOYAMA 2008
September 15-18, 2008

P1-49

STUDY OF A GAS THRUST BEARING WITH SUPPLY GROOVES

Guido BELFORTE, Federico COLOMBO, Terenziano RAPARELLI, Andrea TRIVELLA, Vladimir VIKTOROV

Department of Mechanical Engineering, Politecnico di Torino
Technical University
C.so Duca degli Abruzzi, 24 - 10129 - Torino -Italy
(E-mail: terenziano.raparelli@polito.it)

ABSTRACT

Plane externally pressurized thrust gas bearings for high speed spindles are considered. The behavior of the rotor-bearing system is studied both numerically and experimentally. A numerical model based on Reynolds equation is used to simulate the static and dynamic behavior of the system. Flow rate equation through inlet orifices is coupled with Reynolds equation. The flow rate is calculated by considering an experimentally determined discharge coefficient, that is function of holes diameter and local clearance. To increase stiffness are studied thrust bearings presenting a circumferential groove situated at the same radius of the supply holes. The influence of the groove on stiffness and stability is discussed. Simulations are made to evaluate the influence of supply holes diameter and of axial clearance on bearing characteristics.
Two thrust bearings are studied experimentally. They are composed by a symmetric couple of disks facing the rotor flange. The internal and external diameters of the disks are 52 mm and 110 mm and equipped with 8 holes of diameter 0.35 mm on a circumference of diameter 65 mm. A thrust bearing present a rectangular section circumferential groove, located at the same radius of the orifices, of width 0.7 mm and thickness 10 μm.
Comparisons between simulated and experimental stiffness are presented.

KEY WORDS

Gas, Thrust, Bearing, Grooves

NOMENCLATURE

b	critical ratio = 0.528
C_S	conductance
c_d	discharge coefficient
d_S	supply orifice diameter
F	axial force acting on the rotor (comprehensive of rotor weight)
G	mass flow rate
h	axial clearance
h_0	axial clearance in central position
h_g	groove depth
K	axial stiffness

k_T	temperature coefficient = $\sqrt{293/T^0}$
m	rotor mass
N	number of orifices on each bearing disc
P	absolute pressure
P_S	supply absolute pressure
q	inlet mass flow rate per unit surface
Re	Reynolds number
R^0	gas constant = 287.6 m^2/s^2K
r	radius
r_g	groove radius
r_o	supply holes circumference radius
S	orifice section
T^0	absolute temperature in normal condition
t	time
w_g	groove width
z	axial coordinate
μ	air viscosity
ρ_N	air density in normal condition
ϑ	angular coordinate
ω	rotational frequency

INTRODUCTION

Air bearings are often used in precision systems and high speed spindles for low friction losses and high positioning accuracy. They are applied in linear guideways, thrust bearings and rotating systems. Typical supply systems in case of circular geometries are annular orifices compensated bearings.

The design of such systems is more and more sophisticated and concerns the number and the diameter of supply orifices, the bearing geometry and sometimes the choice of grooves machined on bearing surfaces. The static and dynamic performance of these bearings depend on these parameters. Numerous are the studies on this field intended to optimize either stiffness or air flow rate [1]-[7]. Other works concentrate the study on the micro grooves [8,9] and on the benefits they introduce on the load capacity. It doesn't exist a single procedure that allows to find the best solution, because according to the applications the design requirements are different.

In [10] is presented a theoretical and experimental work on high speed spindle radial air bearings. Figure 1 shows the section of the spindle, composed by the carter 1, the rotor 2 of length 460 mm and diameter 50 mm, the radial bearings 3, the double thrust bearing 4. Each radial bushing presents 16 radial orifices of diameter 0.25 ± 0.01 mm, fabricated with EDM process. Radial clearance is approximately 20 μm.

Air bearings are supplied by ports 5. The rotor is accelerated by the pneumatic turbine 6, supplied by the distributor 7.

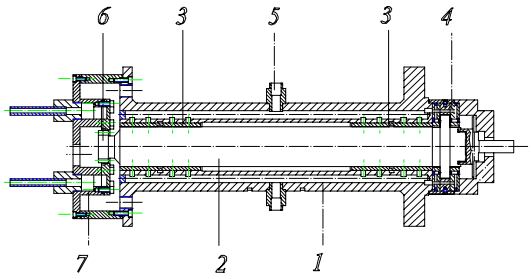

Figure 1 Pneumatic spindle

In this paper is studied the thrust bearing of the above-mentioned spindle with two different thrust geometries. The first solution considers plane disks with supply orifices equispaced, the other one presents a circular groove in correspondence of the supply orifices as well. Are described the geometry of the thrust bearings, the mathematical model, the test rig, the experimental and numerical results in terms of load capacity and stiffness. Then stability is numerically studied.

SCHEME OF THE THRUST BEARING AND NUMERICAL MODEL

Figure 2 shows the principal geometric parameters of the thrust bearing. It is composed by two disks *1* and *2* of inner radius r_i separated by the central ring *3*. Between disks *1* and *2* is present the flange *4*, of radius r_e, jointed to the rotor of radius R. The difference of thickness between ring *3* and flange *4* defines the axial gap $h_1 + h_2$. On each disc *1* and *2* are symmetrically machined N equispaced axial nozzles of calibrated diameter d_S, positioned on a circumference of radius r_o. In case *a* of Figure 2 is visible the supply orifices geometry. In case *b* the disks present a circumferential groove of radius $r_g = r_o$ and rectangular section of width w_g and depth h_g. F is the axial force applied, comprehensive of the rotor weight, z and ϑ are the cylindrical coordinates.

To model the thrust bearing were made the assumptions of isothermal expansion, laminar and viscous flow in the gap. Defining G the air mass flow rate through each supply hole, the time dependent Reynolds' equation (1) [11] in polar coordinates was solved with finite difference method for the two axial gaps.

$$r^2 \frac{\partial}{\partial r}\left(Ph^3 \frac{\partial P}{\partial r}\right) + \frac{\partial}{\partial \vartheta}\left(Ph^3 \frac{\partial P}{\partial \vartheta}\right) + 12\mu R^0 T^0 r^2 q = 6\mu\omega r^2 \frac{\partial(Ph)}{\partial \theta} + 12\mu r^2 \frac{\partial(Ph)}{\partial t} \qquad (1)$$

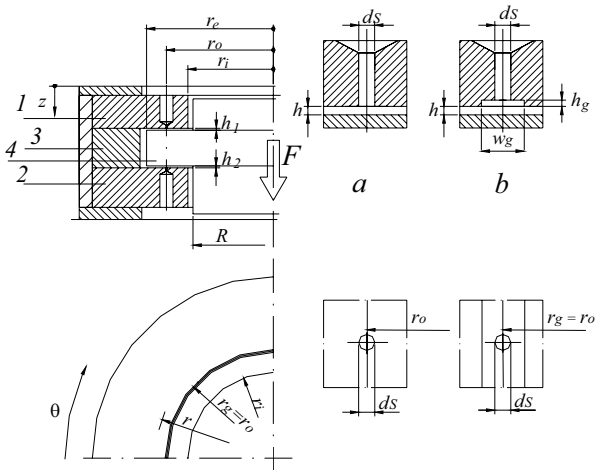

Figure 2 Scheme of thrust bearing

The clearances relative to each bearing disc are:

$$\begin{cases} h_1 = h_0 + z \\ h_2 = h_0 - z \end{cases} \tag{2}$$

where h_0 is the clearance when the rotor flange is centered between the thrust bearing disks.

Term $q = G/(r\,dr\,d\vartheta)$ is the inlet mass flow rate per unit surface and is calculated only in the nodes that coincide with the supply holes. P_S is the absolute supply pressure. Mass flow rate G is calculated in accordance with ISO 6358, where P_c is the supply hole downstream absolute pressure, see equation. (3).

Conductance C_S appearing in the mass flow rate formula is expressed by equation (4), in which S is the cross-section of the simple orifice and c_d is the discharge orifice coefficient. The former depends on local clearance h, on supply port diameter d_S and on Reynolds number Re, calculated with (5) in correspondence of supply port section. The value of c_d was experimentally determined by measuring G and the pressure distribution under the orifice [13]. The equation extrapolated is (6).

$$G = \begin{cases} C_S k_T \rho_N P_S \;, & if \quad 0 < \dfrac{P_c}{P_S} < b \\ C_S k_T \rho_N P_S \sqrt{1 - \left(\dfrac{\frac{P_c}{P_S} - b}{1 - b} \right)^2} & ,if \quad 0 < \dfrac{P_c}{P_S} < b \end{cases} \tag{3}$$

$$C_S = 0.686 \frac{c_d S}{\rho_N \sqrt{R^0 T^0}} \tag{4}$$

$$Re = \frac{4G}{\pi d_S \mu} \tag{5}$$

$$c_d = 0.85 \left(1 - e^{-8.2 \frac{h+h_g}{d_S}} \right) \cdot \left(1 - e^{-0.005\,\mathrm{Re}} \right) \tag{6}$$

In Figure 3 is shown the pressure distribution (expressed in Pa) in case of eight orifices of diameter d_S, supply pressure P_S =0.7 MPa and clearance h_0 =15 μm.

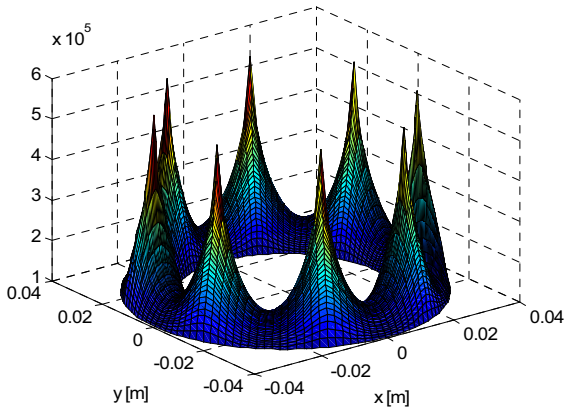

Figure 3 Numerical axial pressure distribution

Static

Calculations were made to obtain the pressure distribution in the thrust bearing at different air clearances h_0. In this case the program solves equations (1) to (5) numerically in time from initial condition $P = P_a$ everywhere and reaches the steady-state solution after a transient. Mass flow rate through the supply holes is calculated iteratively evaluating the hole downstream pressure level p_c from (1), calculating G from (3-4), Re from (5), c_d from (6) and substituting in (3-4) till convergence.

Dynamic

To analyse the step-jump response of the thrust bearing, equations (1 to 5) were solved in time together with the axial spindle equation of motion (7):

$$m\,\ddot{z} + F_t(t) = F(t) \tag{7}$$

in which F_t is the reaction force of the thrust bearing and m is the rotor mass, equal to 7.24 kg. The reaction force is calculated by integrating the pressures P_1 and P_2 present in the axial air gaps h_1 and h_2 over the thrust surfaces:

$$F_t(t) = \int_0^{2\pi} \int_{r_i}^{r_e} (P_2(t) - P_1(t)) r\,dr\,d\theta \tag{8}$$

EXPERIMENTAL SET UP

Figure 4 shows a scheme of the set up to measure load

capacity and stiffness of the double thrust bearing. The carter *1* is mounted vertically on basement *2*. The load devices *3*, *4* are composed by two hollow cylinders containing a calibrated sphere with a clearance of 40 μm. They are positioned radially and axially and they are facing the nose 5. The load on the rotor is applied by pressurizing the inside of the cylinders; its value is obtained by measuring this pressure. For these tests only axial load was applied and without rotation of the spindle ($\omega = 0$). The axial load device allows to load rotor upwards. To load rotor downwards calibrated masses were laid on its top. In this way it was possible to measure the characteristics in both directions of the external load.

Two are the supply air lines: one is dedicated to the bearings, another to the load devices. In the first one is present a reservoir that assures temporarily supply air also in case of failure of the principal supply line. In both are used two high efficiency filters of class 1 that maintain the air clean from micro particles that could choke some orifices.

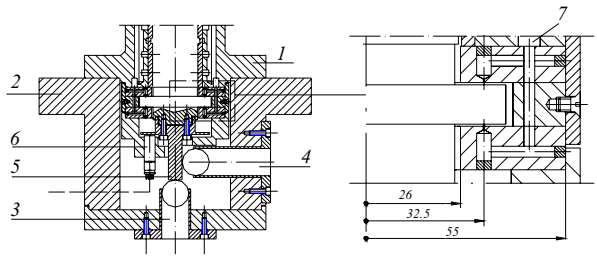

Figure 4 Thrust bearing section

A capacitive displacement transducer *6* with 0.1μm resolution, 500 μm full scale reading and 6 kHz passband was used to measure the axial displacement z . The amplified signal was read on a dedicated conditioning module.

In the same figure is also shown a magnification of the double thrust bearing, where are visible radial and axial supply channels. Supply calibrated holes are fabricated with EDM process. The geometric parameters chosen for the prototypes type *a* and *b* are $N = 8$, $d_S = 0.35 \pm 0.01$ mm, $r_o = 32.5$ mm, $r_i = 26$ mm, $r_e = 38.5$ mm. The nominal axial clearance is $h_0 = 19$ μm. It results measuring axial gap $h_1 + h_2$ like above described using Eq. (2). This value was then compared measuring the axial gap by moving the rotor axially without supply pressure. In this case h_0 is calculated from the rotor axial displacement and it is equal to 13 μm. The difference between the two h_0 values is probably due to geometric tolerance in fabricating the disks of the thrust bearing and on the measure precision.

For the geometry *b* the groove is defined by: $w_g = 0.7$ mm, $h_g = 10$ μm. Figure 5 shows a photo of the grooved disk and the enlargement of a supply hole.

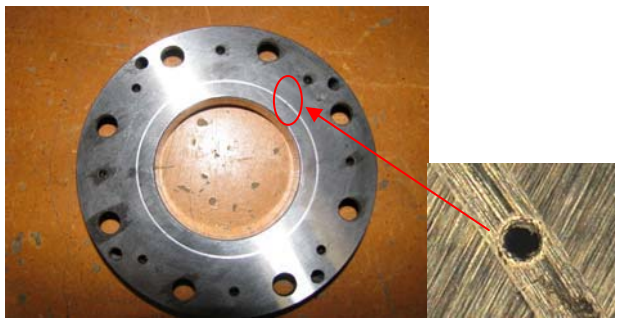

Figure 5 Photo of grooved disk and supply orifice magnification

In Figure 6 are shown the supply air lines of the system: one is dedicated to the bearings, another to the load devices. In the first one is present a reservoir *8* that assures temporarily supply air also in case of failure of the principal supply line. In both are used two high efficiency filters *9* of class 1 that maintain the air clean from micro particles that could choke some orifices.

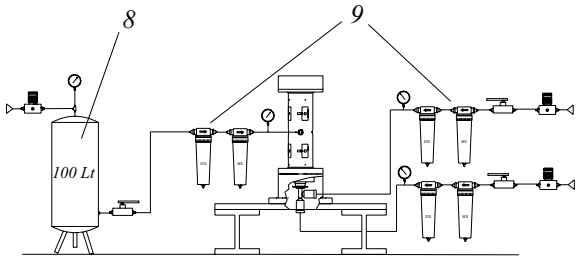

Figure 6 Supply bearing system

RESULTS AND DISCUSSION

Static behavior analysis

Experimental and numerical results are discussed in static behavior considering $d_S = 0.35$ mm, $h_0 = 19$ μm, and different supply pressure P_S (0.3-0.9 MPa) for the two thrust bearings realized ($h_g = 0$ μm, $h_g = 10$ μm). Figures 7 and 8 show the load F v.s. axial displacement experimental diagrams without and with groove.

Positive and negative loads are obtained respectively using the axial load device and applying calibrated mass. The zero displacement point is obtained by applying by the load device an external force opposed to the rotor weight.

Comparing Figures 7 and 8 it is clear that the groove increases stiffness and improves the linearity of the characteristics. It is also verified the simmetry respect the zero.

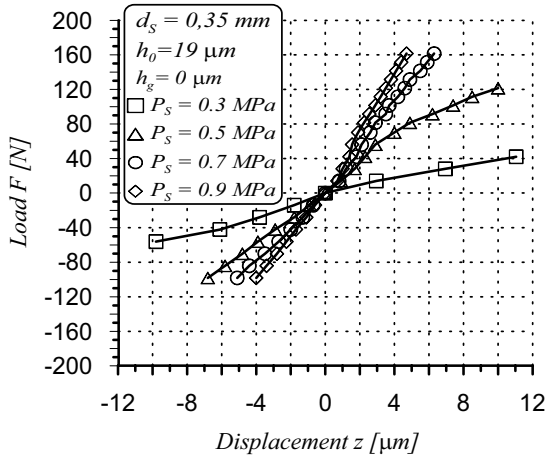

Figure 7 Load v.s. displacement experimental diagram in case of thrust without groove

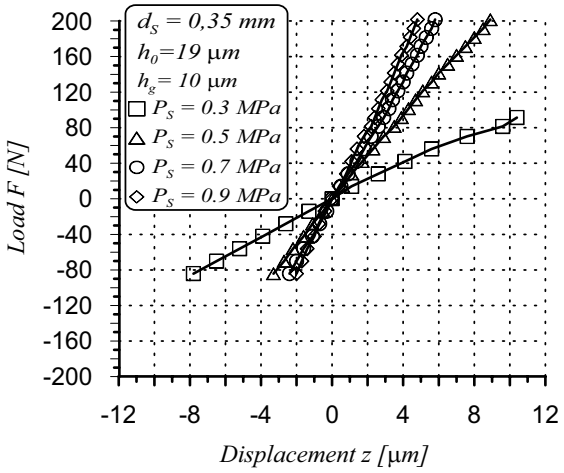

Figure 8 Load v.s. displacement experimental diagram in case of thrust with groove

In Figures 9 and 10 are compared numerical and experimental load carrying capacities respectively at P_S = 0.7 and 0.3 MPa. In particular in Figure 9 calculated stiffness with h_g =10 μm is 40 N/μm, while without groove it is 28 N/μm, that is 30% lower. Numerical results present good linearity in the range $\varepsilon = z / h_0$ =0÷0.4. Experimental stiffness are 6% and 12% lower than numerical ones in case of 10 mm groove and without groove respectively.

In case of P_S =0.3 MPa without groove difference between numerical and experimental results is more evident.

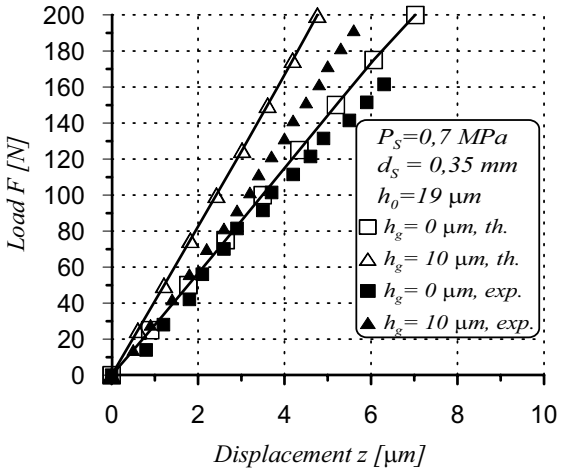

Figure 9 Load v.s. displacement with P_S =0.7 MPa

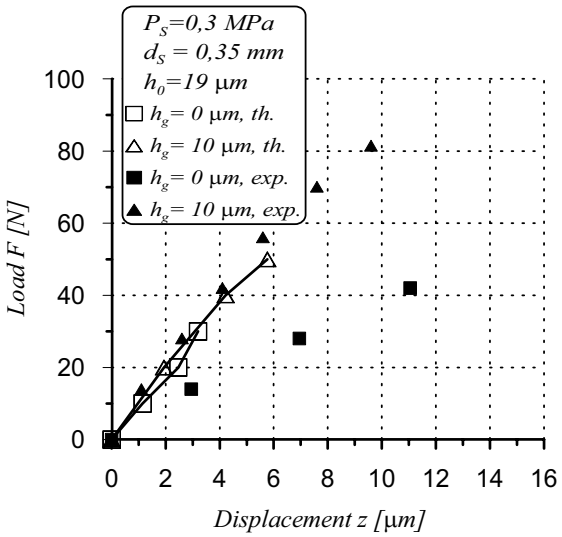

Figure 10 Load v.s. displacement with P_S =0.3 MPa

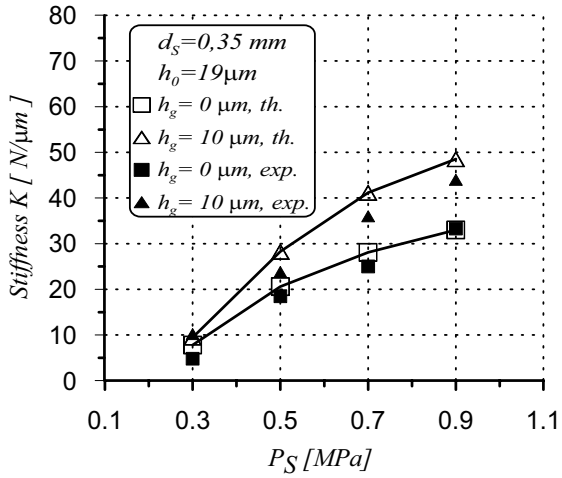

Figure 11 Stiffness v.s. supply pressure P_S

Figure 11 shows a comparison between numerical and experimental stiffness for both thrust bearings at

different supply pressures.
To evaluate stiffness was considered a 4 μm displacement with respect to central position ($z = 0$).

Step response and stability analysis
In this section are shown the dynamic numerical simulations of thrust bearing considering d_S =0.35 mm, h_0 = 19 μm, and supply pressure P_S = 0.7 MPa. Stability is investigated by analyzing the rotor response to a 100 N force step with different groove depth: h_g =0, 10 and 20 μm. In Figure 12 are compared the responses in the three cases, considering the 7.24 kg rotor mass. It is visible that by increasing the groove depth stiffness increases but motion becomes lower damped till instability for h_g =20 μm.

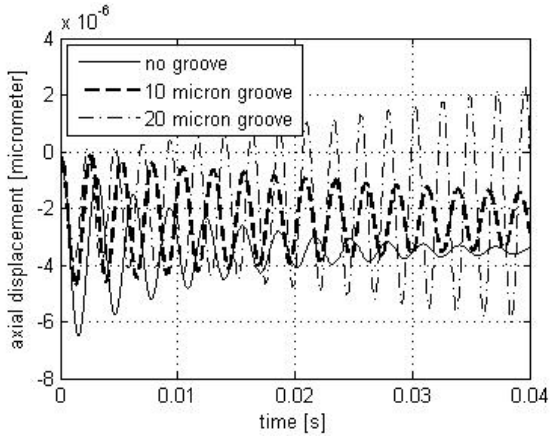

Figure 12 Thrust step response

It was verified that with the 20 μm deep groove the thrust is unstable. So the preferred solution is to adopt a thrust bearing with a groove of 10 μm depth.

CONCLUSIONS

Comparisons between simulated and experimental stiffness and flow rate are shown. Numerical method is suitable to simulate a grooved thrust bearing.
The circular groove increases stiffness, but numerical results show that the groove volume decreases stability.

ACKNOWLEDGEMENTS

The present research was conducted in the LAQ-IBIS with the support of PRIN06 “Study and development of gas bearings for ultra high speed electrospindle” and of FIRB Project “Enabling technologies for multitasking high precision machining of microparts”.

REFERENCES

1. Al-Bender, F. and Van Brussel, H., Tilt Characteristics of Circular Centrally Fed Aerostatic Bearings, Tribology International, 1992, **25**-3, pp.189-197.
2. Yoshimoto, S., Tamura, J. and Nakamura, T., Dynamic Tilt Characteristics of Aerostatic Rectangular Double-Pad Thrust Bearings With Compound Restrictors, Tribology International, 1999, **32**, pp.731-738.
3. Bang, K.G. and Lee, D.G., Thrust Bearing Design for High-Speed Composite Air Spindles, Composite Structures, 2002, **57**, pp.149-160.
4. Shigeka, Y., Makoto, Y. and Kazuyuki, T., Numerical Calculations of Pressure Distributionin the Bearing Clearance of Circular Aerostatic Thrust Bearings With a Single Air Supply Inlet, Transactions of the ASME, 2007, **129**-4, pp.384-390.
5. Belforte, G., Raparelli, T. and Viktorov, V., Theoretical Investigations of Fluid Inertia Effects and Stability of Self-Acting Gas Journal Bearings, ASME Journal of Tribology, 1999, **121**-4, pp. 836-843.
6. Belforte, G., Raparelli, T. and Viktorov, V., Modeling and Identification of Gas Journal Bearings: Self-Acting Gas Bearing Results, ASME J. Tribology, 2002, **124**, pp.716-724.
7. Viktorov, V., Belforte, G. and Raparelli T., Modeling and Identification of Gas Journal Bearings: Externally Pressurized Gas Bearing Results, ASME J. Tribology, 2005, **127**, pp.548-556.
8. Nakamura T, Yoshimoto S., Static tilt characteristics of aerostatic rectangular doublecompound restrictors, Tribology Int. 1996; **2**, pp. 145-152.
9. Chen, M.F. and Lin, Y.T., Static Behavior and Dynamic Stability Analysis of Grooved Rectangular Aerostatic Thrust Bearings by Modified Resistance Network Method, Tribology International, 2002, **35**, pp. 329-338.
10. Belforte, G., Raparelli, T., Viktorov, V., Trivella, A., and Colombo, F., An Experimental Study of High-Speed Rotor Supported by Air Bearings: Test rig and First experimental results. Tribology International, 2006, **39**, pp. 839-845.
11. Grassam, N.S. and Powell J.W., Gas Lubricated Bearings, Butterworths, London, 1964, pp. 135-139.
12. Belforte, G., Colombo, F., Raparelli, T., Trivella, A., and Viktorov, V., Study of a High Speed Electrospindle With Air Bearings, European Conference on Tribology ECOTRIB 2007 Ljubliana, June 12-15, 2007, **2**, pp. 969-982.
13. Belforte, G., Raparelli, T., Viktorov, V. and Trivella, A., Discharge Coefficients of Orifice-Type Restrictor for Aerostatic Bearings, Tribology International, 2007, **40**, pp. 512-521.